Available online at www.sciencedirect.com
ScienceDirect
International Journal of Pharmaceutics 327 (2006) 160–169
INTERNATIONAL JOURNAL OF PHARMACEUTICS
www.elsevier.com/locate/ijpharm

Pharmaceutical Nanotechnology

Effect of nanoparticulate polybutylcyanoacrylate and methylmethacrylate–sulfopropylmethacrylate on the permeability of zidovudine and lamivudine across the *in vitro* blood–brain barrier

Yung-Chih Kuo *, Hung-Hao Chen

Department of Chemical Engineering, National Chung Cheng University, Chia-Yi, Taiwan 62102, Republic of China

Received 24 April 2006; received in revised form 9 July 2006; accepted 17 July 2006
Available online 29 July 2006

Abstract

Effect of size of nanoscaled polybutylcyanoacrylate (PBCA) and methylmethacrylate–sulfopropylmethacrylate (MMA–SPM) on the permeability of zidovudine (AZT) and lamivudine (3TC) across the blood–brain barrier (BBB) was investigated. Also, influence of alcohol on the permeability of AZT and 3TC incorporated with the two polymeric nanoparticles (NPs) was examined. The loading efficiency and the permeability of AZT and 3TC decreased with an increase in the particle size of the two carriers. By employing PBCA NPs, the BBB permeability of AZT and that of 3TC became, respectively, 8–20 and 10–18 folds. Application of MMA–SPM NPs leaded to about 100% increase in the BBB permeability of the two drugs. In the presence of 0.5% ethanol, 4–12% enhancement in the BBB permeability of the two drugs was obtained in the current carrier-mediated system.

Keywords: Permeability; Blood–brain barrier; Zidovudine; Lamivudine; Polybutylcyanoacrylate; Methylmethacrylate–sulfopropylmethacrylate

1. Introduction

Cellular compositions of the blood–brain barrier (BBB) consist of brain-microvascular endothelial cells (BMECs), astroglia, pericytes, microvessel-surrounding macrophages, and basal membranes. Fundamental BBB characteristics arise from the regulations of the cell system. Astrocytes are responsible for the intimate connections among BMECs, neurons, cerebral compartments, and meninges (Raub et al., 1992). However, BMECs actually play the critical role in the development of BBB traits. Also, P-glycoprotein, a BMEC membrane protein, possesses several essential pharmacological functions of drug portage and expulsion (Gelperina et al., 2002). Removal of cyclosporin A and vincristine from brain was concluded to be related to the P-glycoprotein efflux performance (Tsuji and Tamai, 1997). For the animal source of BMECs, endothelia have been mainly separated from bovine and porcine, besides murine (Abbott et al., 1992; Arthur et al., 1987; Tontsch and Bauer, 1989), canine (Gerhart et al., 1988), ovine (Vorbrodt et al., 1994; Vorbrodt and Trowbridge, 1991), and primate (Miller et al., 1992). Bovine BMECs (BBMECs) might be the most satisfactory mammalian cells for constructing the *in vitro* BBB model (Gaillard et al., 2001). The *in vitro* BBMEC culture preserved the *in vivo* BBB features, including cellular homogeneity, tight junction (TJ), existence of specific enzyme markers and antigens corresponding to the antibody factor VIII, and lack of fenestrations and pinocytotic vesicles (Audus and Borchardt, 1986).

For the study of drug transport, absorption, metabolism, and elimination, nucleoside reverse transcriptase inhibitors (NRTIs) have become the standard agents against human immunodeficiency virus (HIV). Relevant data concerning the other two kinds of anti-HIV agents, non-nucleoside reverse transcriptase inhibitors (NNRTIs) and protease inhibitors (PIs), were relatively scarce in the scientific literature. NRTIs such as zidovudine (AZT) (Thomas and Segal, 1997; Masereeuw et al., 1994), didanosine (Hoesterey et al., 1991), and stavudine (Yang et al., 1997) might transport into the central nervous system through

Abbreviations: 3TC, lamivudine; ALE, absolute loading efficiency (%); AZT, zidovudine; BBMEC, bovine brain-microvascular endothelial cells; BMEC, brain-microvascular endothelial cells; MMA–SPM, methylmethacrylate–sulfopropylmethacrylate; NP, nanoparticle; NRTI, nucleoside reverse transcriptase inhibitor; PBCA, polybutylcyanoacrylate; RLE, relative loading efficiency (%)

* Corresponding author. Tel.: +886 5 272 0411x33459; fax: +886 5 272 1206.
E-mail address: chmyck@ccu.edu.tw (Y.-C. Kuo).

0378-5173/$ – see front matter © 2006 Elsevier B.V. All rights reserved.
doi:10.1016/j.ijpharm.2006.07.044

Nomenclature

C_r	drug concentration in receiver chamber (ppm)
ΔC	concentration difference between donor and receiver (ppm)
D	average particle diameter (nm)
P_{BMEC}	permeability of AZT or 3TC across the *in vitro* BBB model (cm/s)
P_e	permeability of AZT or 3TC across BBMECs on PC membrane (cm/s)
P_m	permeability of AZT or 3TC across PC membrane (cm/s)

passive diffusion. Nevertheless, the range of drug concentration reported in the literature caused controversial issues. The shortcomings of AZT are low curative effect via plasma and side effect on marrow intoxication. In an *in vivo* study, it was concluded that only inappreciable amount of AZT permeated into mouse brains (Ahmed et al., 1991). In an assessment of the BBB transport in rabbit, the AZT efflux was five times the AZT influx, and 73% AZT efflux was due to its competition with probenecid (Wong et al., 1993). Although lamivudine (3TC), an NRTI, maintained good absorbability and 80% bioavailability by oral administration, transport of 3TC into cerebrospinal fluid was not facile (Wang et al., 1997).

Colloidal biomaterials can enhance the drug permeability across BBB. Nanoparticulate system not only retained full antiviral activity of AZT (Bender et al., 1994) but also reduced cytotoxicity of AZT (Lobenberg et al., 1997) in an *in vitro* culture of human macrophages. Furthermore, antiviral activity of saquinavir, a PI with poor bioavailability, was enhanced 10-fold by the incorporation with nanoparticles (NPs) (Bender et al., 1996). Polybutylcyanoacrylate (PBCA) NPs can be synthesized by catalytic polymerization of cyanoacrylate monomers over a trace of hydroxyl in an acidic solution. Drugs loaded on PBCA NPs to overcome the BBB limitation included hexapeptide dalargin (Schroeder and Sabel, 1996), dipeptide kytorphin (Schroeder et al., 1998), leuenkephalin (Kreuter et al., 1995), tubocurarine (Alyaudin et al., 1998), and doxorubicin (Gelperina et al., 2000). Thus, PBCA NPs would be qualified NRTI carriers to meliorate the BBB permeability. Methylmethacrylate (MMA) and sulfopropylmethacrylate (SPM) can copolymerize to become methylmethacrylate–sulfopropylmethacrylate (MMA–SPM) NPs. SPM is a strong acid providing permanent negative charge to improve the loading capacity for hydrophilic drugs (Kuo, 2005; Langer et al., 1996). By binding to MMA–SPM, bioavailability of ophthalmic arecaidine propargyl ester was significantly ameliorated (Langer et al., 1997a,b). Thus, MMA–SPM NPs would be proper to bear hydrophilic NRTIs for brain targeting.

Alcohol can transport rapidly across BBB. For anaesthetized dogs, high alcohol concentration could appreciably improve the BBB transportability of sodium fluorescein, which was correlated to the lipid solubility in alcohol (Gulati et al., 1985). For chronically intoxicated rats, the BBB permeability of tyrosine, tryptophan, and DOPA was significantly increased, and the permeability of the three drugs at low alcohol dose (<2 g/kg/day) was higher than that at high alcohol dose (>3.5 g/kg/day) (Borisenko, 1990). Besides, alcohol could physiologically affect the proliferation of astrocytes, leading to cellular hypertrophy and hyperplasia (Mayordomo et al., 1992). Under magnetic resonance observation, acute and chronic alcoholization induced temporary TJ opening (Thompsen et al., 1994). In a study of the BBB transport in rat, sucrose permeability was not noticeably altered by the alcoholic treatment except for starving rats (Philips and Cragg, 1982). Moreover, the BBB permeability of glucose was not apparently varied with the existence of alcohol (Hemmingsen et al., 1980). At low temperature, alcoholization would not influence the amount of Evans blue across BBB (Elmas et al., 2001). The BBB functions were not declined when the alcohol concentration in blood plasma reached anaesthesia (Philips, 1981). Since the above literatures yielded contradictory consequences, it would be worth testing for the effect of alcohol on the transport of NRTIs across BBB. In the present study, effect of particulate diameter of PBCA and MMA–SPM NPs on the loading efficiency of AZT and 3TC was presented. By employing an *in vitro* BBMEC model, the BBB permeability of AZT and 3TC on PBCA and MMA–SPM NPs was evaluated. Influence of medium ethanol on the permeability of AZT and 3TC across BBB was also investigated.

2. Materials and methods

2.1. Reagents and chemicals

Eagle's minimum essential medium (EMEM, Sigma, St. Louis, MO), 2-[4-(2-hydroethyl)-1-piperazine] ethane-sulfonic acid (HEPES, J.T. Baker, Phillipsburg, NJ), penicillin G (Sigma, St. Louis, MO), streptomycin sulfate (Sigma, St. Louis, MO), polymyxin B sulfate (Sigma, St. Louis, MO), amphotericin B (Sigma, St. Louis, MO), Dulbecco's phosphate buffered saline (DPBS, Sigma, St. Louis, MO), sodium hydrogen carbonate (Riedel-de Han, Seelze, Germany), sodium hydroxide (Showa, Tokyo, Japan), hydrochloric acid (Hayashi, Osaka, Japan), protease/dispase (Sigma, St. Louis, MO), Dextran 70,000 (Fluka Biochemika, Buchs, Switzerland), collagenase/dispase (Sigma, St. Louis, MO), fetal bovine serum (Sigma, St. Louis, MO), Percoll (Sigma, St. Louis, MO), trypan blue (Sigma, St. Louis, MO), dimethyl sulfoxide (J.T. Baker, Phillipsburg, NJ), polycarbonate (PC) membrane (with pore diameter of 0.4 μm, Whatman, Clifton, NJ), rat tail collagen (Sigma, St. Louis, MO), acetic acid (Showa, Tokyo, Japan), human fibronectin (Sigma, St. Louis, MO), Kaighn's modified F-12 Ham nutrient mix (Sigma, St. Louis, MO), and heparin sodium (Sigma, St. Louis, MO) were used for isolation, counting, viability assessment, preservation, and cultivation of BBMECs. Anhydrous methyl alcohol (HPLC grade, Mallinckrodt Baker, Phillipsburg, NJ), Triton-X-100 (Acros, Geel, Belgium), anti-human von Willebrand factor VIII (Sigma, St. Louis, MO), anti-rabbit IgG with FITC conjugate (Sigma, St. Louis, MO), formalin solution (Sigma, St. Louis, MO), and anti-ZO-1 (Zymed, South San Francisco, CA)

were employed for immunohistochemical fluorescent staining of BBMEC culture. Butylcyanoacrylate (BCA, Sicomet, Hanover, Germany), D-mannitol (Sigma, St. Louis, MO), ammonium persulfate (APS, Sigma, St. Louis, MO), methyl methacrylate (MMA, Fluka Chemica, Buchs, Switzerland), sulfopropyl methacrylate potassium salt (SPM, Aldrich, Milwaukee, WI), and filter paper (Toyo Roshi, Tokyo, Japan) were used for synthesis and purification of PBCA and MMA–SPM NPs. Acetonitrile (BDH Laboratory Supplies, Poole, England) were applied to high performance liquid chromatography (HPLC) of AZT (3′-azido-3′-deoxythymidine, GlaxoWellcome, London, England) and 3TC (2′,3′-dideoxy-3′-thiacytidine, GlaxoWellcome, London, England). Ultrapure water was obtained from an Ultropure Reverse Osmosis and Nanopure Infinity Ultrapure System (Barnstead, Dubuque, IA).

2.2. Isolation, cultivation and characterization of BBMECs

BBMECs were isolated from several bovine brains by enzymatic disaggregation reported previously (Kuo and Chung, 2005) with minor modifications. The steps for BBMEC isolation are summarized in Fig. 1(a). Summarized procedures for fluorescent characterization of BBMECs are shown in Fig. 1(b). The fluorescent images of BBMECs and TJ were observed under a phase contrast fluoromicroscope (Axioskop 2 plus, Zeiss, Munchen-Hallbergmoos, Germany).

2.3. Nanoparticle preparation

PBCA NPs and MMA–SPM copolymer NPs were synthesized, respectively, by emulsion polymerization and free radical polymerization (Kuo, 2005). The average particle diameter of the two kinds of NPs in every batch was controlled by the rate of magnetic stirring during reaction. The distribution of particle diameter and the cumulant *Z*-average diameter of the lyophilized drug-loaded NP powders were determined by a zeta sizer 3000 (Malvern Instruments, Worcs, UK) with photo correlation spectroscopy. The images of electron microscopy were obtained by a field emission scanning electron microscope (FE-SEM, JSM-6330 TF, Joel, Tokyo, Japan).

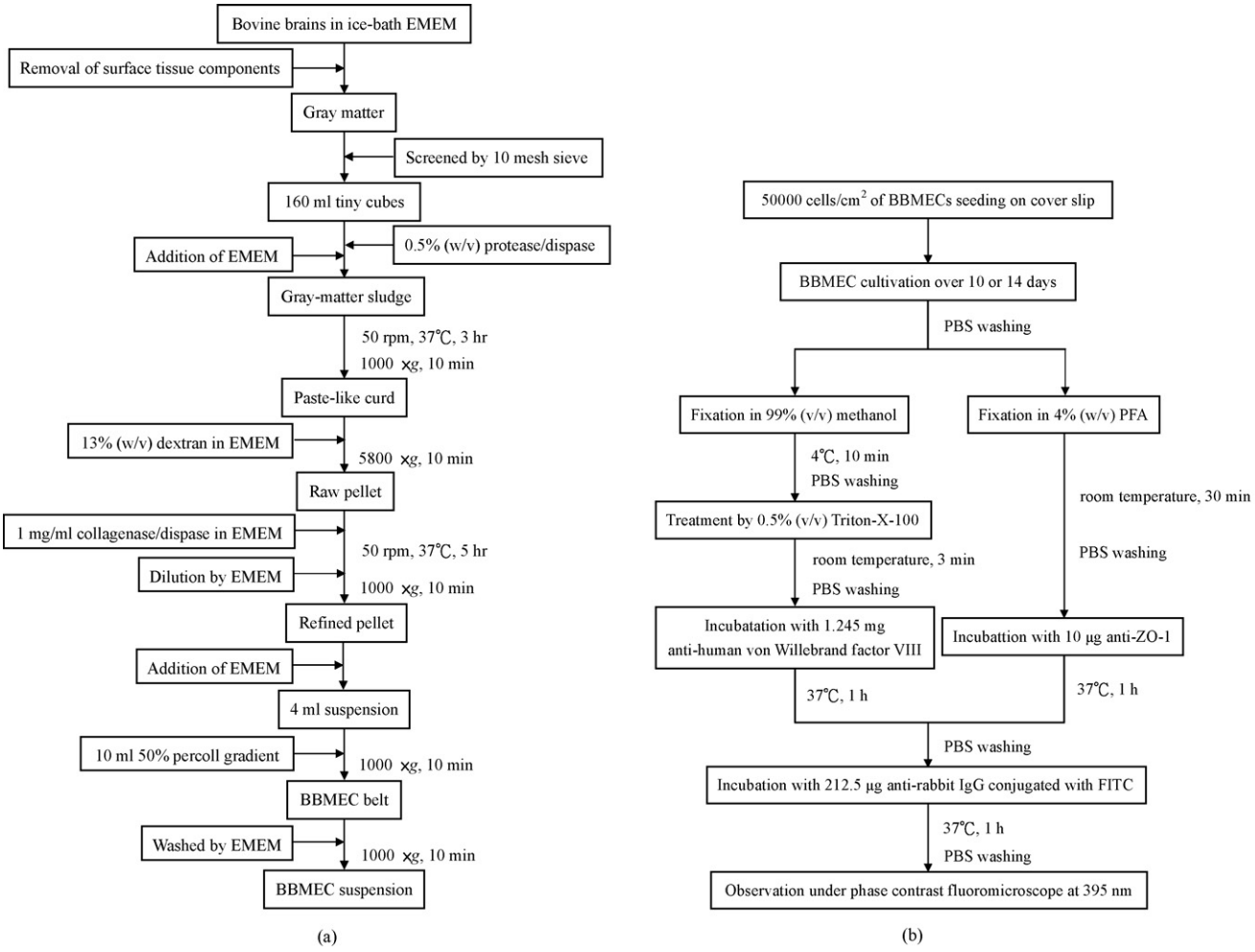

Fig. 1. (a) Summarized procedures for BBMEC isolation from bovine brains; (b) summarized procedures for fluorostaining of BBMEC culture by immunohistochemical method; (c) experimental scheme for the evaluation of drug permeability across the *in vitro* BBB model; (d) calculation algorithm for the permeability data.

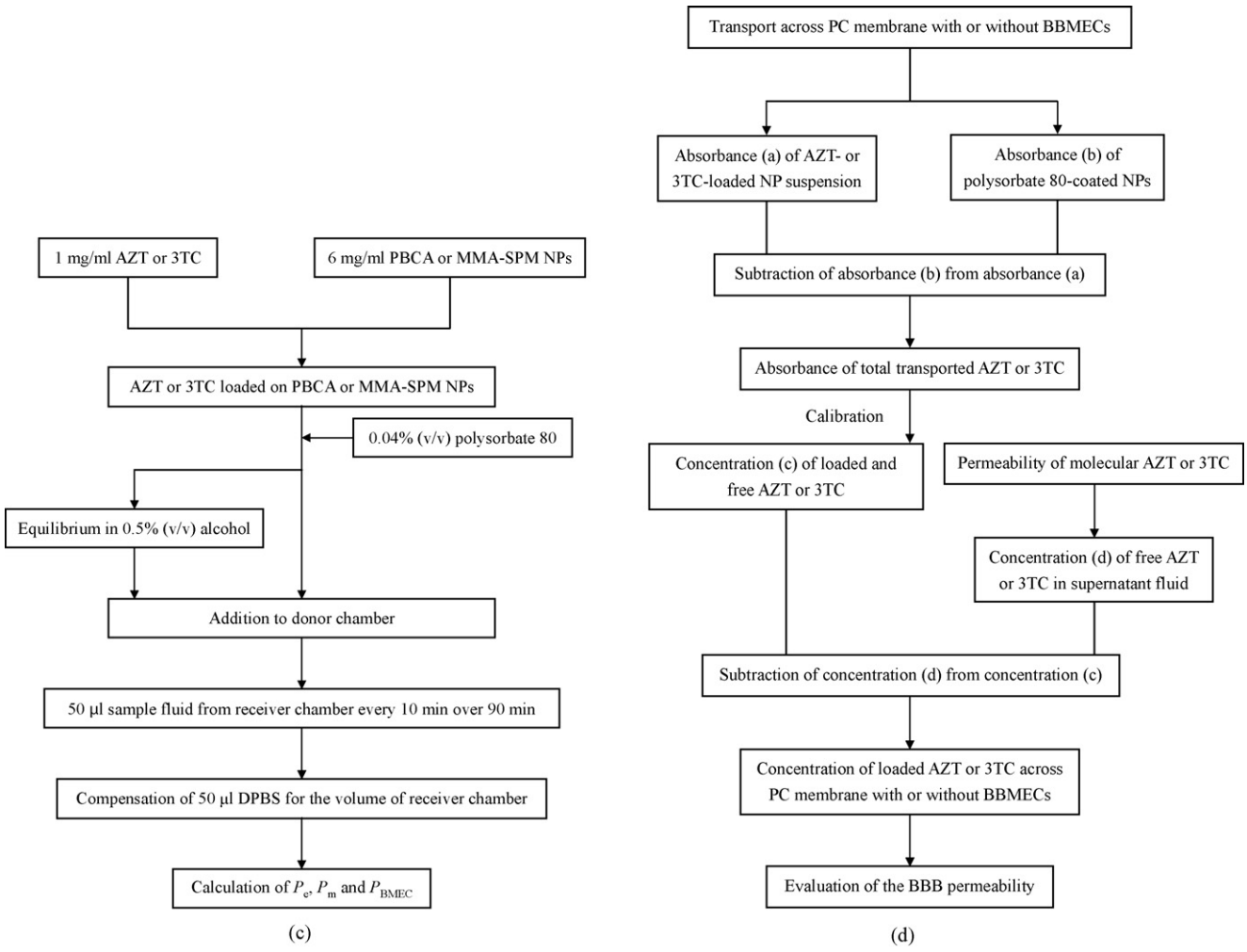

Fig. 1. (*Continued*).

2.4. Loading efficiency of AZT and 3TC

Method for loading and quantitative analysis of drugs on NP surfaces was reported previously (Kuo, 2005) with minor modifications. Ultraviolet absorbance of AZT and 3TC was determined by a UV–vis spectrophotometer (Bio-Tek Instruments, Winooski, VT) at 250 nm (Simon et al., 2001). Non-adsorbed AZT or 3TC in supernatant was separated by HPLC (Jasco, Tokyo, Japan) with a reverse phase BDS Hypersil C-18 column (Thermo Hypersil-Keystone, Bellefonte, PA) warmed by a heater (Alltech, Derrfield, IL) at 37 °C. The relative loading efficiency (RLE) and the absolute loading efficiency (ALE) of AZT and 3TC are defined, respectively, by

$$\mathrm{RLE}(\%) = \frac{\text{total weight of AZT or 3TC} - \text{weight of unloaded AZT or 3TC}}{\text{total weight of AZT or 3TC}} \times 100;$$

$$\mathrm{ALE}(\%) = \frac{\text{total weight of AZT or 3TC} - \text{weight of unloaded AZT or 3TC}}{\text{total weight of NP carriers}} \times 100$$

2.5. Permeability of AZT and 3TC across BBB

Experimental set-up for estimation of the *in vitro* BBB permeability is described below. Briefly, PC membrane with or without BBMECs was fastened between two chambers, filled up with 14 ml pure DPBS at 37°C. Donor chamber contains 1000 ppm drug. Fifty microliters of sample fluid was drawn out from receiver chamber every 10 min and analyzed by a UV–vis spectrophotometer. After ultracentrifugation, supernatant fluid was detected by a UV–vis spectrophotometer (UV-2075 Plus, Jasco, Tokyo, Japan) following HPLC. Duration of each run of the transport study was 90 min. 0.5% ethanol in DPBS was applied in the study of the alcoholic effect. Experimental scheme and evaluation algorithm for the transport data are summarized in Fig. 1(c) and (d), respectively. Transport amounts of molecular AZT and 3TC were estimated by independent experiments for their permeability. Amount of AZT or 3TC transported in NP-incorporated state was determined by subtracting the free AZT or 3TC out of the overall transport drug. The permeability coefficient of AZT and 3TC across BMEC monolayer, P_{BMEC},

can be calculated by (Glynn and Yazdanian, 1998):

$$\frac{1}{P_{\mathrm{BMEC}}} = \frac{1}{P_{\mathrm{e}}} - \frac{1}{P_{\mathrm{m}}}, \qquad P_i = \frac{J/A}{\Delta C} = V_{\mathrm{r}}\left(\frac{\mathrm{d}C_{\mathrm{r}}/\mathrm{d}t}{A\Delta C}\right), \quad i = \mathrm{e\ or\ m}$$

where P_{e} and P_{m} are, respectively, the permeability coefficient of drug across PC membrane with BBMECs and that without BBMECs, J/A, ΔC, V_{r}, C_{r}, t, and A denote respectively, the mass flux of drug from donor chamber into receiver chamber, the concentration difference between the two chambers, the volume of receiver chamber, the drug concentration in receiver chamber, the time, and the transport surface area.

2.6. Statistics

Unless otherwise indicated, all data presented here were mean ± standard deviation. Statistical significance for the data comparison was assessed using a one-way analysis of variance (ANOVA) followed by Tukey's HSD test.

3. Results and discussion

3.1. Morphology of BBMEC culture and NPs

Fig. 2 shows the immunofluorescent results of BBMEC culture. As revealed in Fig. 2(a) and (b), BBMECs presented not only aggregation but also regular compact array, which was one of the traits of cerebral microvessel endothelia. Aligned structure was seldom observed for endothelia obtained from other tissues, such as lung, adipose, and aorta (Craig et al., 1998). As presented in Fig. 2(c), shimmering TJ emerged in the contact region among BBMECs. Dark spaces were the cells, which lacked the specific anti-ZO-1 staining. Furthermore, the fluorescent TJ contour around BBMECs was similar to spiderweb, which was consistent with the literature result (Wu et al., 2003). Thus, the currently cultured BBMEC monolayer exhibited confluent aspect and TJ feature, demonstrating the main physiological function of *in vivo* BBB was preserved. Since astrocytes induce relatively integrated tight intercellular junction among BMECs, co-culture of BMECs and astrocytes may yield even ideal BBB properties.

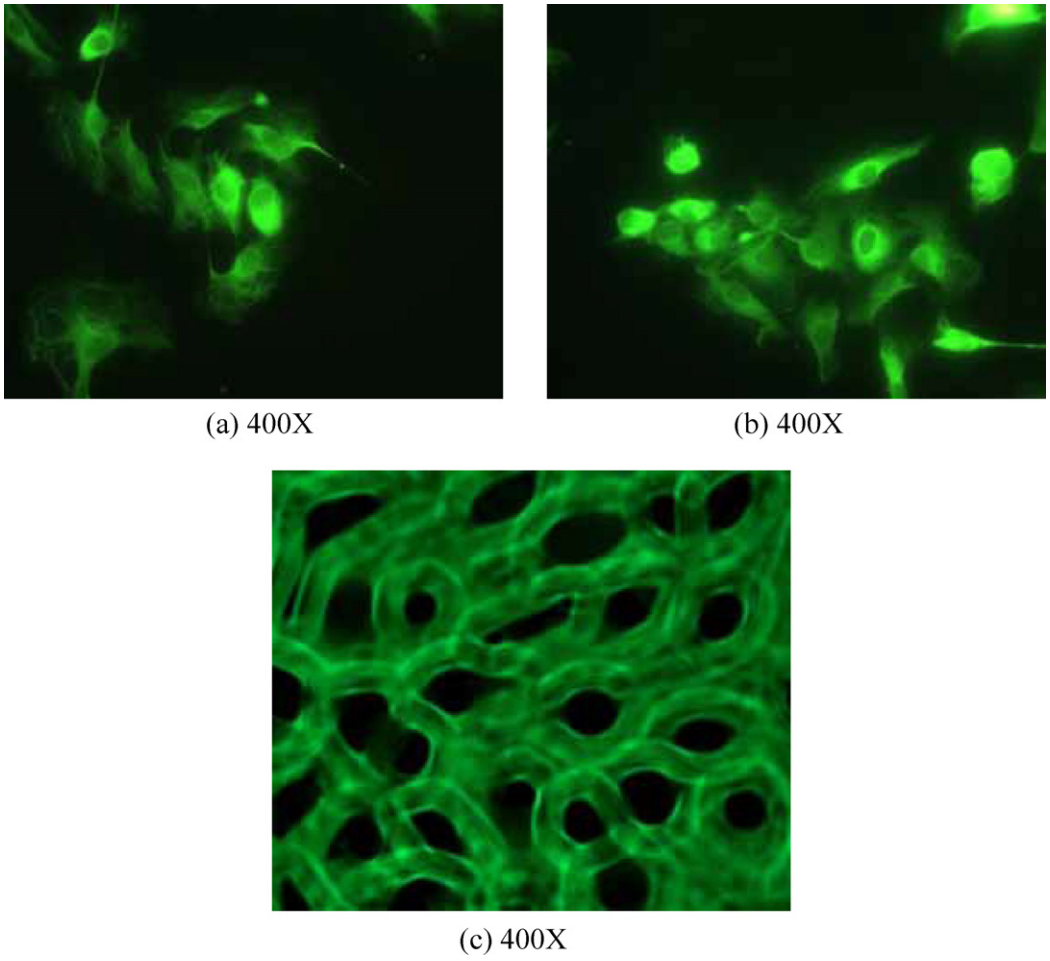

Fig. 2. Immunofluorescent images of BBMEC culture. (a) and (b) for BBMECs over 10-day cultivation and (c) for TJ among adjacent BBMECs over 14-day cultivation.

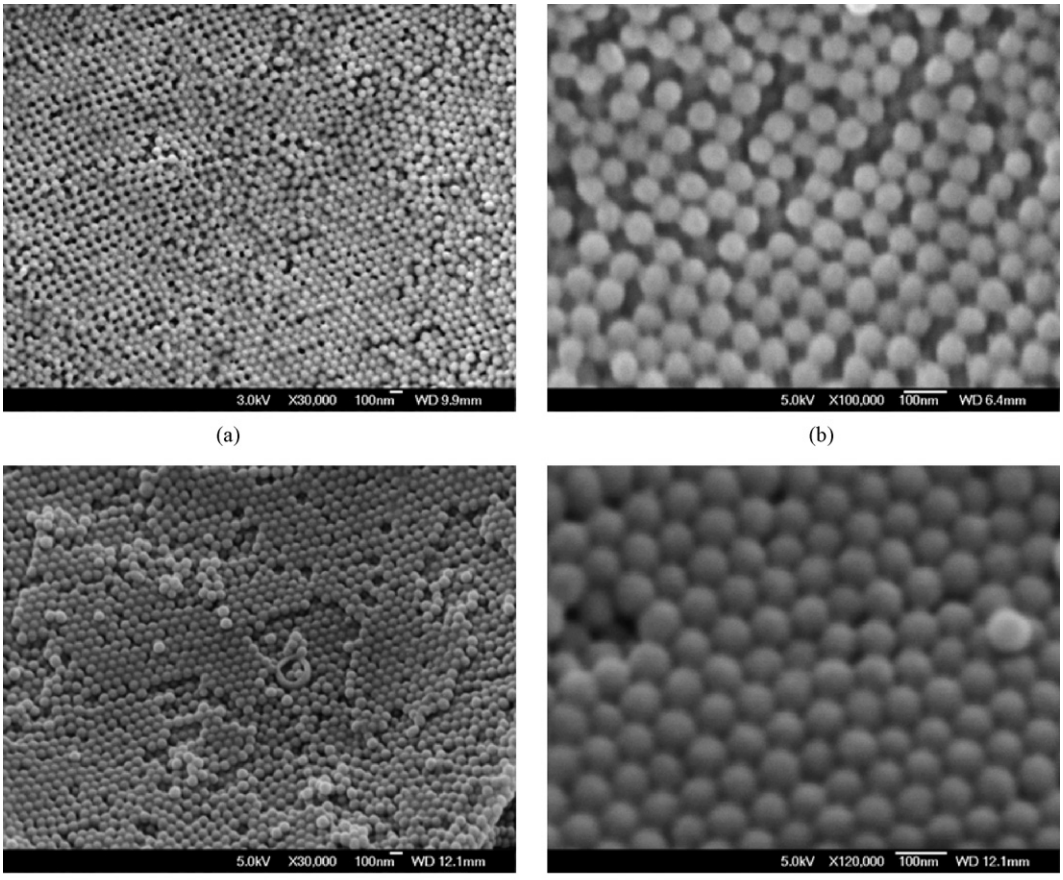

Fig. 3. FE-SEM micrographs of AZT-loaded polymeric NPs. (a) and (b) for PBCA; (c) and (d) for MMA–SPM.

Fig. 3 presents FE-SEM images of AZT-loaded PBCA and MMA–SPM NPs. Nearly monodispersed NPs with spheroidal shape were obtained, as suggested in Fig. 3. AZT loading could only slightly interfere in the NP morphology because the amount of drug adsorbed on the carrier surfaces was much smaller than the buck NP entity. Although BCA polymerized rapidly in acidic solution, agglomeration of the water-insoluble oligomers within the polymer matrix might affect particulate exteriors (Behan et al., 2001). Moreover, separation between PBCA NPs was observed, indicating the existence of particular inter-particulate repulsion. On the contrary, closely layer-by-layer piled MMA–SPM NPs with tiny gap were obtained. Since the synthesis rate of MMA–SPM NPs was relatively slow, compact spheres with the layer structure could be resulted from the chemical reaction process.

3.2. RLE and ALE of AZT and 3TC

Fig. 4 shows the variations in RLE and ALE of AZT and 3TC as a function of the average particle diameter (D) of PBCA NPs. As revealed in this figure, RLE and ALE of both drugs on PBCA NPs slightly decreased as D increased. The rationale behind this result was that a larger D produced a smaller specific surface area of NPs and yielded a lesser amount of adsorbed drugs. RLE and ALE of 3TC were higher than those of AZT. This was because 3TC was more hydrophilic than AZT, and the superficial zone of PBCA NPs was coated with a layer of hydrophilic dextran 70,000 (Douglas et al., 1985).

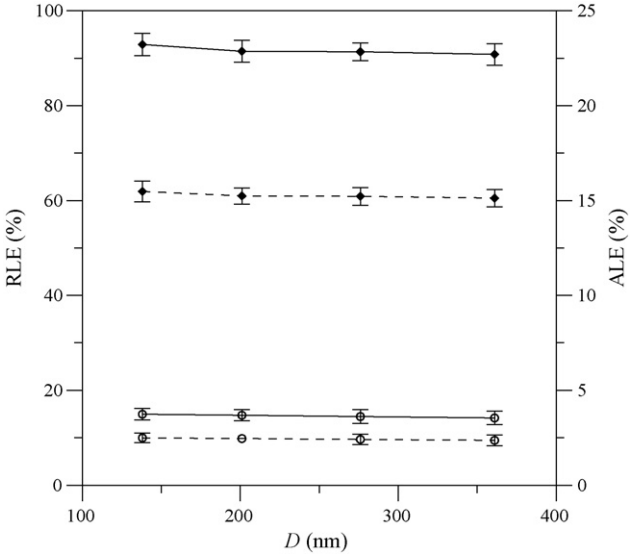

Fig. 4. Variations in RLE and ALE of AZT and 3TC as a function of D of PBCA NPs. Key: (◯) for AZT; (♦) for 3TC; solid curve for RLE; dashed curve for ALE.

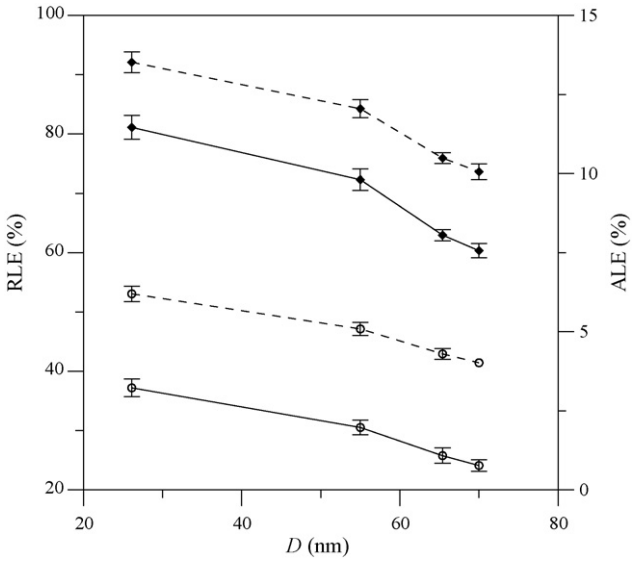

Fig. 5. Variations in RLE and ALE of AZT and 3TC as a function of D of MMA–SPM NPs. Key: same as Fig. 4.

Variations in RLE and ALE of AZT and 3TC as a function of D of MMA–SPM NPs are exhibited in Fig. 5. Since SPM generates ionogenic functional groups, drugs can be prevalently loaded on MMA–SPM NPs via ionic regulation. As compared with the results shown in Fig. 4, RLE and ALE on MMA–SPM NPs reduced apparently as D increased. This could be interpreted by the fact that a larger MMA–SPM carrier possessed fewer effective adsorption sites per unit mass. Also, MMA–SPM NPs commonly induces strong affinity to drugs of high hydrophilicity. Hence, RLE and ALE of 3TC were higher than those of AZT, as indicated in Fig. 5.

Amount of AZT loaded on PBCA NPs was fewer than that on MMA–SPM NPs. For hydrophilic materials, loading capacity on MMA–SPM NPs was usually higher than that on PBCA NPs (Kuo, 2005). AZT belonged to the hydrophilic pharmaceuticals as compared with PI and NNRTI (Glynn and Yazdanian, 1998). Attractive force between the negatively charged MMA–SPM NPs and the N–H group of AZT enhanced affinity of AZT to MMA–SPM surfaces. On the contrary, amount of 3TC loaded on MMA–SPM NPs was fewer than that on PBCA NPs. This was owing to that the active sites for 3TC adsorption on the dextran-coated PBCA surfaces were more than those on the ionized MMA–SPM NPs.

3.3. Permeability of AZT- and 3TC-loaded NPs

Fig. 6(a) and (b) shows the variations in the permeability (P_e and P_m) of AZT and those of 3TC as a function of D of PBCA NPs, respectively. Variations in P_e and P_m of AZT and those of 3TC as a function of D of MMA–SPM NPs are presented in Fig. 7(a) and (b), respectively. As displayed in these figures, P_e and P_m decreased as D increased. Since the mass-transfer resistance to PC membrane increased with D, a larger D generated a smaller P_m. Transports through BBMEC monolayer on PC membrane for NPs with a larger D were also more difficult than those with a smaller D. Hence, a larger D yielded a smaller

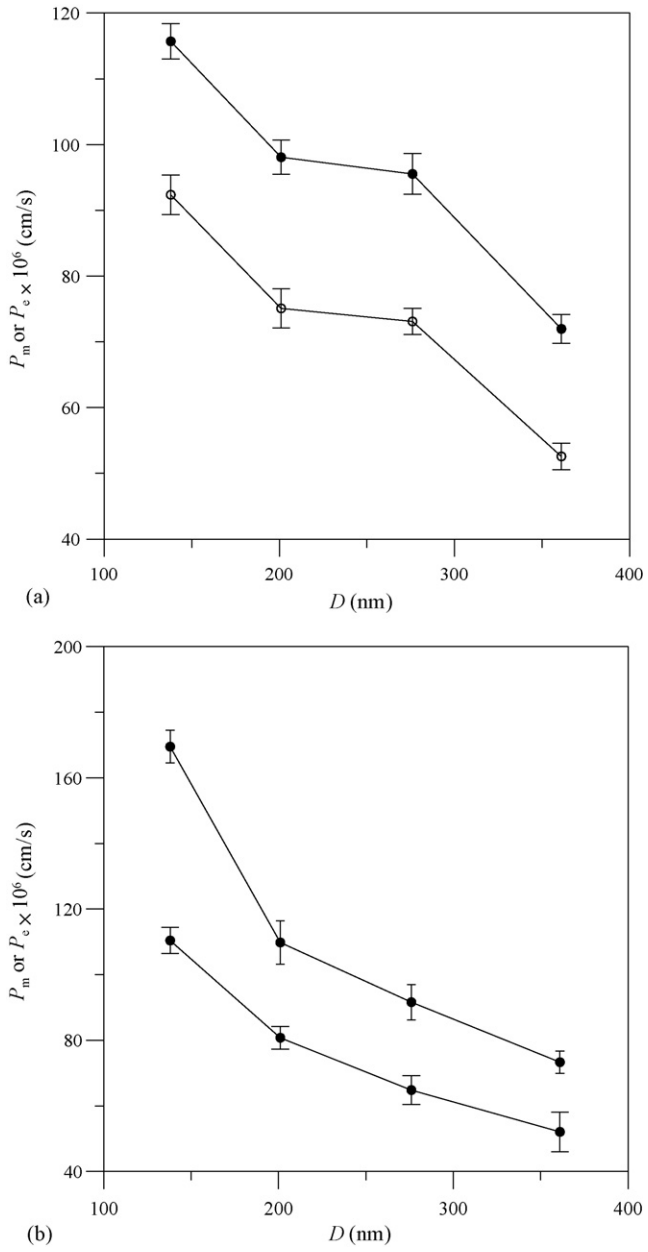

Fig. 6. (a) Variations in P_e and P_m of AZT loaded on PBCA NPs as a function of D of PBCA NPs. Key: (◯) for P_e; (●) for P_m. (b) Variations in P_e and P_m of 3TC loaded on PBCA NPs as a function of D of PBCA NPs. Key: same as (a).

P_e. As revealed in Fig. 7(a) and (b), D of MMA–SPM NPs was less than 70 nm and effect of D increment on the reduction in P_m was more noticeable than that in P_e. This implied that small variation in D of MMA–SPM NPs might cause inappreciable influence on the transport of AZT and 3TC across BBMECs.

Fig. 8 presents the variations in P_{BMEC} as a function of D of PBCA NPs. As indicated in this figure, P_{BMEC} of AZT and 3TC decreased when D increased. In the present study, P_{BMEC} of AZT was $23.2 \pm 1.1 \times 10^{-6}$ cm/s and P_{BMEC} of 3TC was $16.8 \pm 1.3 \times 10^{-6}$ cm/s. These values were close to the results reported in the literature (Glynn and Yazdanian, 1998). Fig. 8 indicates that P_{BMEC} of AZT and P_{BMEC} of 3TC in PBCA system without alcohol became, respectively, about 8–20 and 10–18

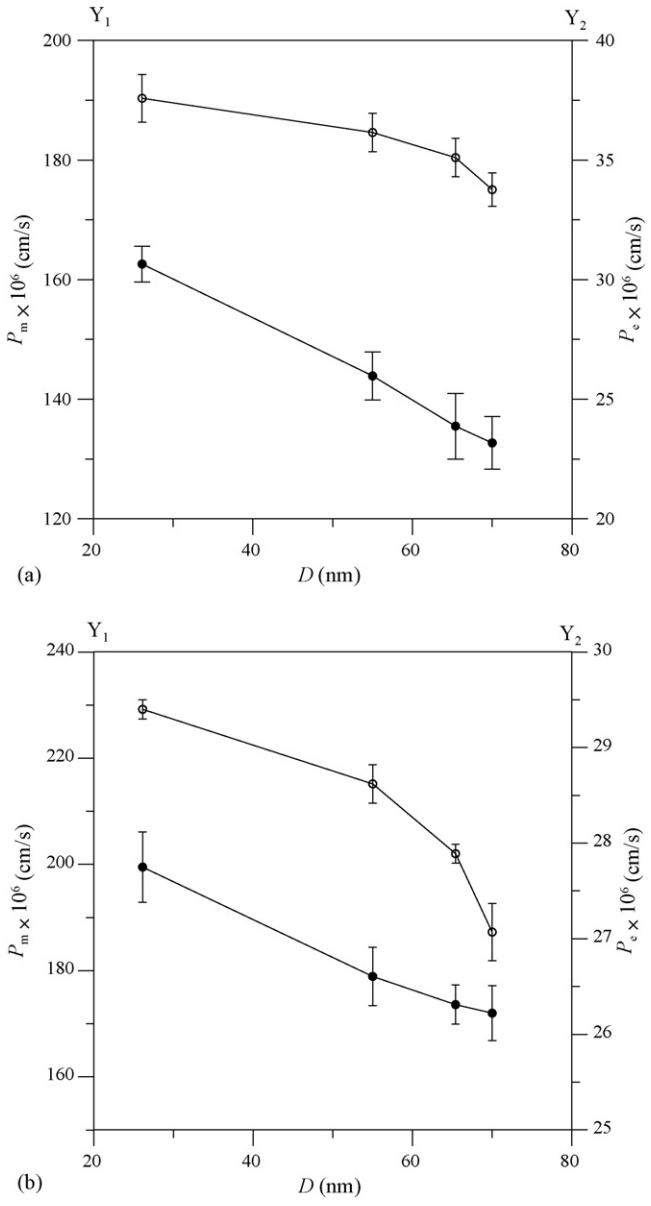

Fig. 7. (a) Variations in P_e and P_m of AZT loaded on MMA–SPM NPs as a function of D of MMA–SPM NPs. Key: (◯) for P_e using Y_2 axis; (●) for P_m using Y_1 axis. (b) Variations in P_e and P_m of 3TC loaded on MMA–SPM NPs as a function of D of MMA–SPM NPs. Key: same as (a).

folds. In a BBB study on intravenously injected mice, the concentration of amitriptyline increased 10 folds in the brain while the drug was loaded on PBCA NPs (Schroeder et al., 1998). Also, C_r varied linearly with time, and the drug concentration in donor chamber was sustained at 1000 ppm, which was much larger than C_r. Thus, ΔC was about a constant. Under a constant ΔC, P_{BMEC} was proportional to the temporal variation in C_r and to C_r at a fixed transport time.

Variations in P_{BMEC} as a function of D of MMA–SPM NPs are shown in Fig. 9. As revealed in the solid curves of Fig. 9, P_{BMEC} of AZT and 3TC on MMA–SPM NPs was about two times that without NP incorporation. Since BBMECs were capable of absorbing polymethylmethacrylate particles (Borchard et al., 1994), the concentration gradient of AZT and 3TC between

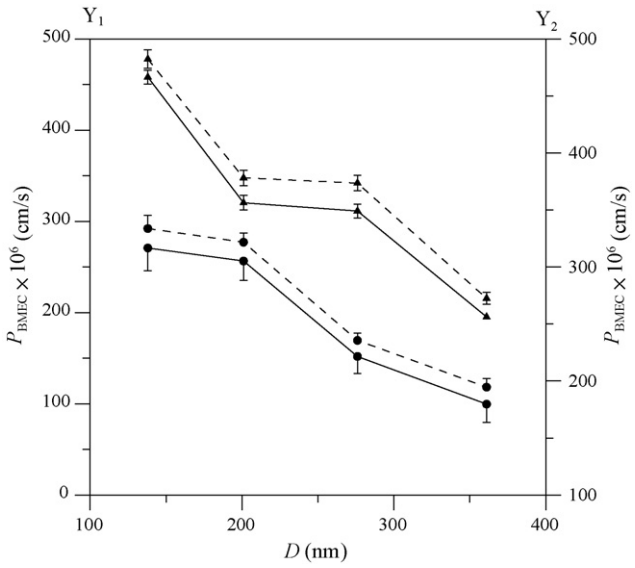

Fig. 8. Variations in P_{BMEC} as a function of D of PBCA NPs. (▲) for AZT using Y_1 axis; (●) for 3TC using Y_2 axis; solid curve: without alcohol; dashed curve: with 0.5% alcohol.

BBMEC monolayer and receiver chamber could be raised by the cellular absorption of MMA–SPM NPs.

How NPs improve drug transport across BBB has not been completely clear. Three possible mechanisms described below might explain why NPs were beneficial to drug delivery into the brain. (i) Prolonged interaction interval between drug-loaded NPs and BMECs elevated the concentration gradient between blood and the brain (Schroeder et al., 1998). Thus, driving force of the passive diffusion increased. (ii) Polysorbate 80 covering on the periphery of NPs was able to be absorbed (Kreuter et al., 1995). BMECs belong to reticuloendothelial cells with phagocytic and endocytotic abilities. For this reason, large peptides

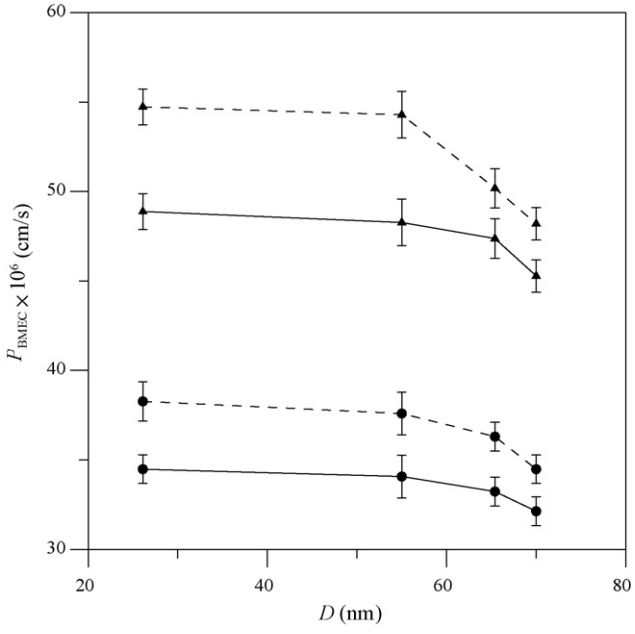

Fig. 9. Variations in P_{BMEC} as a function of D of MMA–SPM NPs. (▲) for AZT; (●) for 3TC; solid curve: without alcohol; dashed curve: with 0.5% alcohol.

or pharmaceuticals can invoke polysorbate 80-filmed NPs for improved delivery into the brain. Inside BMECs, drug diffused into the cerebrum after desorption from NP surfaces (Kreuter, 2001). (iii) Degraded NPs improved drug absorption (Lenaerts et al., 1984). Through the second mechanism, it could be explicated that P_{BMEC} of AZT was larger than P_{BMEC} of 3TC even if RLE of 3TC was higher than RLE of AZT. Note that drug lipophilicity dominated the released AZT and 3TC into receiver chamber.

Comparing Fig. 8 with Fig. 9, P_{BMEC} of AZT and 3TC on PBCA NPs was appreciably larger than that on MMA–SPM NPs. The main rationale behind this consequence was the electrical repulsion between negative charged MMA–SPM NPs and BBMECs (Kuo and Lin, 2006). Endocytosis of MMA–SPM NPs might also lead to a reduction in trans-endothelia electrical resistance. Hence, transport of MMA–SPM NPs was retarded due to the electrostatics. On the other hand, PBCA NPs was positively charged (Kuo and Lin, 2006), rendering attraction between NPs and cells. Furthermore, degraded products of PBCA would be more influential than those of MMA–SPM for drug absorbability.

3.4. Influence of alcohol on P_{BMEC} of AZT and 3TC

0.15% (w/v) ethanol concentration in plasma caused alcohol-induced tipsy situation, and the lethal concentration of ethanol in plasma was 0.5% (w/v). In PBCA/ethanol system, P_{BMEC} of AZT and P_{BMEC} of 3TC increased 4–8 and 5–8%, respectively, as revealed in Fig. 8. Fig. 9 suggests that P_{BMEC} of AZT and P_{BMEC} of 3TC enhanced, respectively, 6–12 and 7–11% in MMA–SPM/ethanol system.

The main reason for these results was temporary unfolding of TJ among BMECs by alcoholic treatment (Thompsen et al., 1994). Besides, BBMECs were in DPBS without nutritional ingredient during the permeability study. Starving BBMECs in conjugation with alcohol destroyed the BBB integrity (Philips and Cragg, 1982). Also, alcohol effect on P_{BMEC} promotion in MMA–SPM system was greater than that in PBCA system. Note that the size of MMA–SPM NPs was smaller than that of PBCA NPs. Hence, the mass-transfer resistance to the temporary TJ unfolding of the former would be smaller than that of the latter.

4. Conclusions

In summary, the loading efficiency and the permeability of AZT and 3TC on PBCA NPs and MMA–SPM NPs were investigated. Influence of ethanol on the transport of AZT- and 3TC-loaded PBCA NPs and MMA–SPM NPs was also presented. The loading efficiency and the permeability of the two drugs decreased with an increase in NP diameter. On PBCA NPs, the BBB permeability of AZT and that of 3TC enhanced, respectively, 8–20 and 10–18 times. By application of MMA–SPM NPs, about duplicate BBB permeability of AZT and 3TC was obtained. Alcohol caused perceptible enhancement (*ca* 4–12%) in the BBB permeability of the two drugs loaded on the two NP carriers. This implied that addition of alcohol in the pharmaceutical formulation would cause positive effect on the BBB delivery. The present BBB model could be extended to the study of drug–carrier relation by infrared spectroscopy and carrier–cell interaction by confocal microscopy. Also, influence of physiological and physiochemical conditions on NP biodegradation could be further examined.

Acknowledgment

This work is supported by the National Science Council of the Republic of China.

References

Abbott, N.J., Hughes, C.C., Revest, P.A., Greenwood, J., 1992. Development and characterization of a rat brain capillary endothelial culture: towards an in vitro blood–brain barrier. J. Cell Sci. 103, 23–37.

Ahmed, A.E., Jacob, S., Loh, J.P., Samra, S.K., Nokta, M., Pollard, R.B., 1991. Comparative disposition and whole-body autoradiographic distribution of [2-^{14}C]azidothymidine and [2-^{14}C]thymidine in mice. J. Pharmacol. Exp. Ther. 257, 479–486.

Alyaudin, R.N., Tezikov, B.E., Ramge, P., Kharkevich, D.A., Begley, D.J., Kreuter, J., 1998. Significant entry of tubocurarine into the brain of rats by adsorption to polysorbate-80 coated polybutylcyanoacrylate nanoparticles: an in situ brain perfusion study. J. Microencapsul. 15, 67–74.

Arthur, F.E., Shiver, R.R., Bowman, P.D., 1987. Astrocyte-mediated induction of tight junctions in brain capillary endothelium: and efficient in vitro model. Dev. Brain Res. 36, 155–159.

Audus, K.L., Borchardt, R.T., 1986. Characterization of an in vitro blood–brain barrier model system for studying drug transport and metabolism. Pharm. Res. 3, 81–87.

Behan, N., Birkinshaw, C., Clarke, N., 2001. Poly *n*-butyl cyanoacrylate nanoparticles: a mechanistic study of polymerization and particle formation. Biomaterials 22, 1335–1344.

Bender, A., von Briesen, H., Kreuter, J., Ducan, I.B., Rubsamen-Waigmann, H., 1996. Efficiency of nanoparticles as carrier system for antiviral agents in human immunodeficiency virus-infected human monocytes/macrophages in vitro. Antimicrob. Agents Chemother. 40, 1467–1471.

Bender, A., Schafer, V., Steffan, A., Royer, C., Kreuter, J., Rubsamen-Waigmann, H., von Briesen, H.V., 1994. Inhibition of HIV in vitro by antiviral drug-targeting using nanoparticles. Res. Virol. 145, 215–220.

Borchard, G.K., Audus, L., Shi, F., Kreuter, J., 1994. Uptake of surfactant-coated poly(methyl methacrylate) nanoparticles by bovine brain microvessel endothelial cell monolayers. Int. J. Pharm. 110, 29–35.

Borisenko, S.A., 1990. Effects of drugs on blood–brain barrier permeability in rats chronically intoxicated by ethanol. Ann. Ist. Super Sanita 26, 39–42.

Craig, L.E., Spelman, J.P., Strandberg, J.D., Zink, M.C., 1998. Endothelial cells from diverse tissues exhibit differences in growth and morphology. Microvasc. Res. 55, 65–76.

Douglas, S.J., Illum, L., Davis, S.S., 1985. Particle size and size distribution of poly(butyl 2-cyanoacrylate) nanoparticles II. Influence of stabilizers. J. Colloid Interf. Sci. 103, 154–163.

Elmas, I., Kucuk, M., Kalayci, R.B., Cevik, A., Kaya, M., 2001. Effects of profound hypothermia on the blood–brain barrier permeability in acute and chronically ethanol treated rats. Forensic Sci. Int. 119, 212–216.

Gaillard, P.J., Voorwinden, L.H., Niesen, J.L., Ivanov, A., Atsumi, R., Engman, H., Ringbom, C., de Boer, A.G., Breimer, D.D., 2001. Establishment and functional characterization of an in vitro model of the blood–brain barrier, comprising a co-culture of brain capillary endothelial cells and astrocytes. Eur. J. Pharm. Sci. 12, 215–222.

Gelperina, S.E., Khalansky, A.S., Skidan, I.N., Smirnova, Z.S., Bobruskin, A.I., Severin, S.E., Turowski, B., Zanella, F.E., Kreuter, J., 2002. Toxicological studies of doxorubicin bound to polysorbate 80-coated poly(butyl cyanoacrylate) nanoparticles in healthy rats and rats with intracranial glioblastoma. Toxicol. Lett. 126, 131–141.

Gelperina, S.E., Smirnova, Z.S., Khalansky, A.S., Skidan, I.N., Bobruskin, A.I., Kreuter, J., 2000. Chemotherapy of brain tumors using doxorubicin bound to polysorbate 80-coated nanoparticles. In: Proceedings of the Third World Meeting on APV/APGI, Berlin, Germany, pp. 441–442.

Gerhart, D.Z., Broderius, M.A., Drewes, L.R., 1988. Cultured human and canine endothelial cells from brain microvessel. Brain Res. Bull. 21, 785–793.

Glynn, S.L., Yazdanian, M., 1998. In vitro blood–brain barrier permeability of nevirapine compared to other HIV antiretroviral agents. J. Pharm. Sci. 87, 306–310.

Gulati, A., Nath, C., Shanker, K., Srimal, R.C., Dhawan, K.N., Bhargava, K.P., 1985. Effect of alcohols on the permeability of blood–brain barrier. Pharmacol. Res. Commun. 17, 85–93.

Hemmingsen, R., Hertz, M.M., Bolwig, T.G., 1980. Integrity of blood–brain barrier during ethanol intoxication and withdrawal in the rat: normal glucose transfer and permeability to Na^+ and Cl^-. Stoke 11, 141–144.

Hoesterey, B.L., Galinsky, R.E., Anderson, B.D., 1991. Dose dependence in the plasma pharmacokinetics and uptake kinetics of 2′,3′-dideoxyinosine into brain and cerebrospinal fluid of rats. Drug Metab. Dispos. 19, 907–912.

Kreuter, J., 2001. Nanoparticulate systems for brain delivery of drugs. Adv. Drug Deliv. Rev. 47, 65–81.

Kreuter, J., Alyautdin, R.N., Kharkevich, D.A., Ivanov, A.A., 1995. Passage of peptides through the blood–brain barrier with colloidal polymer particles (nanoparticles). Brain Res. 674, 171–174.

Kuo, Y.C., Lin, T.W., 2006. Electrophoretic mobility, zeta potential, and fixed charge density of bovine knee chondrocytes, methylmethacrylate–sulfopropylmethacrylate, polybutylcyanoacrylate, and solid lipid nanoparticles. J. Phys. Chem. B 110, 2202–2208.

Kuo, Y.C., 2005. Loading efficiency of stavudine on polybutylcyanoacrylate and methylmethacrylate–sulfopropylmethacrylate copolymer nanoparticles. Int. J. Pharm. 290, 161–172.

Kuo, Y.C., Chung, C.Y., 2005. Transport of zidovudine- and lamivudine-loaded polybutylcyanoacrylate and methylmethacrylate–sulfopropylmethacrylate nanoparticles across the in vitro blood–brain barrier: characteristics of the drug-delivery system. J. Chin. Inst. Chem. Eng. 36, 627–638.

Langer, K., Stieneker, F., Lambrecht, G., Mutschler, E., Kreuter, J., 1997a. Methylmethacrylate sulfopropylmethacrylate copolymer nanoparticles for drug delivery. Part II: Arecaidine propargyl ester and pilocarpine loading and in vitro release. Int. J. Pharm. 158, 211–217.

Langer, K., Mutschler, E., Lambrecht, G., Mayer, D., Troschau, G., Stieneker, F., Kreuter, J., 1997b. Methylmethacrylate sulfopropylmethacrylate copolymer nanoparticles for drug delivery. Part III: evaluation as drug delivery system for ophthalmic applications. Int. J. Pharm. 158, 219–231.

Langer, K., Marburger, C., Berthold, A., Kreuter, J., Stieneker, F., 1996. Methylmethacrylate sulfopropylmethacrylate copolymer nanoparticles for drug delivery. Part I: preparation and physiochemical characterization. Int. J. Pharm. 137, 67–74.

Lenaerts, V., Couvreur, P., Christiaens-Leyh, D., Joiris, E., Roland, M., Rollmann, B., Speiser, P., 1984. Degradation of poly(isobutylcyanoacrylate) nanoparticles. Biomaterials 5, 65–78.

Lobenberg, R., Araujo, L., Kreuter, J., 1997. Body distribution of azidothymidine bound to nanoparticles after oral administration. Eur. J. Pharm. Biopharm. 44, 127–132.

Masereeuw, R., Jaehde, U.M., Langemeijer, W., de Boer, A.G., Breimer, D.D., 1994. In vitro and in vivo transport of zidovudine (AZT) across the blood–brain barrier and the effect of transport inhibitors. Pharm. Res. 11, 324–330.

Mayordomo, F., Renau-Piqueras, J., Megias, L., Guerri, C., Iborra, F.J., Azorin, I., Ledig, M., 1992. Cytochemical and stereological analysis of rat cortical astrocytes during development in primary culture: effect of prenatal exposure to ethanol. Int. J. Dev. Biol. 36, 311–321.

Miller, D.W., Audus, K.L., Borchardt, R.T., 1992. Application of cultured endothelial cells of the brain microvasculature in the study of the blood–brain barrier. J. Tissue Cult. Meth. 14, 217–224.

Philips, S.C., Cragg, B.G., 1982. Weakening of the blood–brain barrier by alcohol-related stresses in the rat. J. Neurol. Sci. 54, 271–278.

Philips, S.C., 1981. Does ethanol damage the blood–brain barrier? J. Neurol. Sci. 50, 81–87.

Raub, T.J., Kuentzel, S.L., Sawada, G.A., 1992. Permeability of bovine brain microvessel endothelial cells in vitro: barrier tightening by a factor released from astroglioma cells. Exp. Cell Res. 199, 330–340.

Schroeder, U., Sommerfeld, P., Ulrich, S., Sabel, B.A., 1998. Nanoparticle technology for delivery of drugs across the blood–brain barrier. J. Pharm. Sci. 87, 1305–1307.

Schroeder, U., Sabel, B.A., 1996. Nanoparticles, a drug carrier system to pass the blood–brain barrier, permit central analgesic effects of i.v. dalagrin injections. Brain Res. 710, 121–124.

Simon, V.A., Thiam, M.D., Lipford, L.C., 2001. Determination of serum levels of thirteen human immunodeficiency virus-suppressing drugs by high-performance liquid chromatography. J. Chromatogr. A 913, 447–453.

Thomas, S.A., Segal, M.B., 1997. The passage of azidodeoxythymidine into and within the central nervous system: does it follow the parent compound, thymidine? J. Pharmacol. Exp. Ther. 281, 1211–1218.

Thompsen, H., Kaatsch, H., Asmus, R., 1994. Magnetic resonance imaging of the brain during alcohol absorption and elimination: a study of the rising tide phenomenon. Blutalkohol 31, 178–185.

Tontsch, U., Bauer, H.C., 1989. Isolation characterization and long-term cultivation of porcine and murine cerebral capillary endothelial cells. Microvasc. Res. 37, 148–161.

Tsuji, A., Tamai, I., 1997. Blood–brain barrier function of P-glycoprotein. Adv. Drug Deliv. Rev. 25, 287–298.

Vorbrodt, A.W., Trowbridge, R.S., Dobrogowska, D.H., 1994. Cytochemical study of the effect of aluminium on cultured brain microvascular endothelial cells. Histochem. J. 26, 119–126.

Vorbrodt, A.W., Trowbridge, R.S., 1991. Ultrastructural study of transcellular transport of native and cationized albumin in cultured goat brain microcascular endothelium. J. Neurocytol. 20, 998–1006.

Wang, J., Su, S.F., Dresser, M.J., Schaner, M.E., Washington, C.B., Giacomini, K.M., 1997. Na(+)-dependent purine nucleoside transporter from human kidney: cloning and functional characterization. Am. J. Physiol. 273, F1058–F1065.

Wong, S.L., Van, B.K., Sawchuk, R.J., 1993. Distributional transport kinetics of zidovudine between plasma and brain extracellular fluid/cerebrospinal fluid in the rabbit: investigation of the inhibitory effect of probenecid utilizing microdialysis. J. Pharmacol. Exp. Ther. 264, 899–909.

Wu, Z., Hofman, F.M., Zlokovic, B.V., 2003. A simple method for isolation and characterization of mouse brain microvascular endothelial cells. J. Neurosci. Meth. 130, 53–63.

Yang, Z., Brundage, R.C., Barbhaiya, R.H., Sawchuk, R.J., 1997. Microdialysis studies of the distribution of stavudine into the central nervous system in the freely-moving rat. Pharm. Res. 14, 865–872.